Engineering and Technology Journal
Journal homepage: https://etj.uotechnology.edu.iq

Optimization of mechanical and biocompatible properties of ZnOs-fiber membranes

Dalia M. Jomaa*, Abbas Kh. Hussien, Jamal J. Dawood

Materials Engineering Dept., University of Technology-Iraq, Alsina'a street, 10066 Baghdad, Iraq.
*Corresponding author Email: dalia.m.gomaa@uotechnology.edu.iq

HIGHLIGHTS

- Bio-composite materials were fabricated for wound healing in three concentrations.
- Biodegradable polymers were used to create electrospun fibers.
- A blend of polyvinyl alcohol and chitosan, incorporated with nanoparticles, was used to modify mechanical properties.

ARTICLE INFO

Handling editor: Mustafa H. Al-Furaiji

Keywords:

Taguchi method

Zinc oxide nanoparticles

Mechanical properties

Mlectro-spun fibers

Wound healing

ABSTRACT

This study uses electro-spinning techniques to create a poly(vinyl alcohol)-chitosan-zinc oxide nanoparticles (PVA+CS)+ZnO NPs system in three concentrations of ZnO for application as composite nanofibers for wound treatment applications and Employing the Taguchi technique to optimize the mechanical characteristics via a four-level experimental design process (L16). Numerous techniques have been utilized to characterize the nanofibrous scaffolds: contact angle measurement, cytotoxicity testing, proliferation testing, evaluation of antimicrobial activity, Fourier Transform Infrared Spectroscopy (FTIR), Field Emission Scanning Electron Microscopy (FESEM), Energy Dispersion X-ray Spectroscopy (EDX), and a comparative experimental study involving the determination of hardness using the Nanoindentation method for (PVA+CS)+ZnO. The ideal combination for adding ZnO as nanoparticles was found to be (PVA+CS)+0.6 ZnO, with a flow rate of 0.5 mL/hr, an applied voltage of 18 kV, and a needle tip-to-collector distance of 15 cm (position). This resulted in the smallest fiber diameter (48 nm) with a smooth and uniform distribution. As a consequence, (PVA+CS)+ZnO can be regarded as non-toxic in accordance with the criteria. The methyl thiazole tetrazolium (MTT) assay was used to evaluate the cell viability of L929 (cell cultures for skin). It significantly affects cell viability, achieving 50% in less than 24 hours, which means cell growth through 24 hours is necessary for embryonic development, tissue repair, and regulation of cell division in case of wound healing. Exhibiting findings of inhibition zone diameter in antibacterial activity test exceeding 20 mm. According to the results, (PVA+CS)+0.6 ZnO's hydrophilic properties showed a well-connected porous structure and made it easier for nutrients and oxygen to be exchanged, encouraging cellular activity. After evaluating the mechanical characteristics of each specimen, the main determinants of these characteristics are determined using a Taguchi orthogonal array L16 design. The results of this study suggest that (PVA+CS)+0.6 ZnO could be a good biomedical material for skin tissue engineering applications.

1. Introduction

Researchers are becoming increasingly interested in innovative materials due to the recent creation of nanofibers with diameters less than 100 nm. These materials show promise in various fields, including biotechnology, electronics, optics, sensors, coatings, tissue engineering, biomedicine, and textiles and membranes [1]. More than 100 synthetic and natural polymers have been employed to produce fibers using electrospinning. Among the synthetic polymers that are often utilized are nylon 6, 6, poly (ethylene oxide), poly (vinyl alcohol), poly (urethane), and poly (methyl methacrylate) [2]. On the other hand, biodegradable polymers such as collagen, poly (lactic acid), and chitosan (CS) have been used in electrospinning; CS is particularly notable due to its antibacterial characteristics.With its antibacterial, antifungal, and antioxidant properties, CS is a non-toxic, biodegradable polymer that promotes faster wound healing and blood coagulation control [3]. PVA is an artificial polymer that has existed for more than 90 years. PVA is made when polyvinyl acetate is saponified, and because of its ability to form films, it has long been mixed with other natural polymers. Due to its inherent characteristics, PVA does not fully dissolve in water [4].

http://doi.org/10.30684/etj.2024.145042.1650
Received 16 December 2023; Received in revised form 08 February 2024; Accepted 13 February 2024; Available online 07 April 2024
2412-0758/University of Technology-Iraq, Baghdad, Iraq

The ZnO nanoparticles' UV-blocking, antibacterial, and antimicrobial properties are outstanding. This is why the textile industry understands that zinc is an important trace element found in abundant quantities in every organ and tissue of the human body. Zinc plays a crucial role in protein and nucleic acid production, hematopoiesis, and neurogenesis [5]. ZnO NPs are significantly safer than other metal oxide NPs and have great biological applications. Only a few examples are the treatment of cancer, the supply of medications, bacteria, and diabetes. Additionally, it may help treat inflammation, wound healing, and bioimaging [6].

The Taguchi experimental design method is a statistical technique that aims to minimize the number of tests required to analyze the impact of different parameters on a product's quality and quantity. Additionally, this technique effectively filters out the key elements that influence the reaction while excluding those with little significance, thereby determining the optimal environment. The Taguchi parameter design approach is cost-effective for enhancing manufacturing processes and achieving stringent quality objectives without incurring additional costs. The signal-to-noise ratio (S/N ratio) is used to evaluate how much effect noise components have on the desired features of a system or signal. Using an orthogonal design of array (OA) allows for analyzing many variables while minimizing the required tests. The signal-to-noise (S/N) ratio evaluation involves three performance criteria: smaller-the-better, larger-the-better, and nominal-the-better. The S/N ratio consolidates the diverse data points within an experimental context, contingent upon the investigated character [6].

Gutha et al.[7] performed a study to investigate the effects of combining (CS+PVA)+ZnO on antibacterial and wound healing properties. The aim was to develop a more effective and convenient material for use in the biomedical field. To achieve this, a mixture of chitosan/PVA solution and zinc oxide nanoparticles was prepared by suspending them in water. (CS+PVA)+ZnO exhibits high antibacterial properties against Escherichia coli and Staphylococcus aureus germs, as demonstrated by both in vitro and in vivo experiments. The (CS+PVA)+ZnO dressings accelerated wound healing based on an in vivo study in mice's skin . Shaghayegh Baghaie et al. studied the effects of using different concentrations of CS and ZnO when preparing the PVA+St+CS polymer hydrogel membrane. The inclusion of nanostructured zinc oxide (ZnO) leads to a reduction in the size and number of all pores. The tensile strength dropped with increased chitosan % and increased with adding ZnO. By augmenting the quantity of chitosan, the water vapor transmission rate escalates. The cell viability exceeded 87%, indicating that PVA/St/Cs/ZnO hydrogel membrane extracts exhibit minimal toxicity towards L929 fibroblast cells. The hydrogel membranes containing PVA/St with a 10% concentration of Cs and nZnO exhibited the most effective antibacterial activity. On the 14th day, the wound healing efficacy of hydrogel without nZnO was 95%, whereas the wound treated with a hydrogel containing nZnO showed a healing efficacy of 96%. In comparison, the control group exhibited a wound-healing efficacy of 79% [3]. The researchers M. Abbas et al. employed The CS+PVA membranes fabricated and embedded with bioactive agents obtained from the C.procera root extract. These membranes were then used for wound healing in rabbits. The swelling, biodegradability, and surface properties of the CS+6PVA membranes were observed to be influenced by the concentration of the extracts (ranging from 25% to 75%) loaded onto the membranes. The reduction of the wounds was monitored for 12 days [8]. Kazharskaia Mariia et al. examined the effect of a recently produced blend of chitosan-van hydrogels and CNCs, which included EGF(epidermal growth factor) as a dressing agent, on enhancing wound healing. The researchers noticed that the prepared hydrogels exhibited acceptable cell survival and non-toxic properties. In summary, the study demonstrated that this nanocomposite system has the potential to be a highly effective wound dressing material and might be applied in various applications within the domains of biomedicine and tissue engineering, particularly to heal skin wounds [9]. The authors of the study are Davood Kharaghani and colleagues. The study involved the creation of antibacterial wound dressings using hybrid nanofibers composed of polyvinyl alcohol/chitosan (CS+PVA+nHA) with the addition of silver nanoparticles (AgNPs), silver/copper nanoparticles (Ag+CuNPs), and copper nanoparticles (CuNPs) through an in-situ electrospinning method. The results indicated that Cs/PVA/nHA nanofibers effectively incorporated metallic nanoparticles, resulting in enhanced antibacterial properties and forming a membrane with good biocompatibility and no toxicity, which is a good sign for cell attachment and biocompatibility [10].

Reid et al.,[11] examined the effect of four different electrospun scaffolds with increasing fiber diameters ranging from 0.75 to 6 µm were electrospun. The largest (6 µm) fiber diameter increased cell infiltration compared to the three other morphologies. Briefly, the electrospun fibers were spun as one continuous fiber onto an aluminum foil-covered 8 cm diameter rotating mandrel in an environment of 18–24 °C and 40/60% relative humidity. The electrospinning parameters used to spin each set of fibers include employing needle pore between (0.4-0.8 mm), flow rate (1.2-6 ml/h), the distance between the needle tip and substrate (12 cm), and voltage (32KV maximum limit).

Nevertheless, previous experimental research has focused on employing biomaterials to promote wound healing. However, none of the previous experimental research used a bio nanocomposite material with three concentrations that possess excellent biocompatibility and optimization of mechanical properties by using Taguchi to fabricate a membrane for wound healing.

The objective of this study is to prepare a composite membrane by incorporating polyvinyl alcohol (PVA) and chitosan (CS) with the addition of zinc oxide nanoparticles (ZnO NPs). And investigate the effect of varying concentrations of ZnO NPs on the biocompatibility and mechanical properties of the membrane. The Taguchi method will also be applied to design the experiments, analyze the influence of various parameters, and be optimized to screen significant factors affecting mechanical properties.

2. Experimental section

2.1 Materials

Chitosan (CS), having a molecular weight (MW) of 161 g/mol and a density (of 0.2 g/cm^3), is procured from Glenham (United Kingdom) for utilization in the present investigation. The poly (vinyl alcohol) with a molecular weight of 67,000 g/mol, density (0.22 g/cm^3) product of Germany, packed in the UK by ME Scientific Engineering, acetic acid (98-100% purity from

Merck) product of USA, and nano zinc oxide with a molecular weight of 81.3 g/mol, density (5.6 g/cm^3) are procured from Sky Spring Nanomaterials, a supplier based in the United States.

2.2 Preparation PVA-CS-ZnO NPs electrospun fibers

The first step for preparing the nanofiber membrane by electrospinning device began with preparing a solution containing eight-weight percent polyvinyl alcohol (PVA) made by dissolving PVA in distilled water at 60 degrees Celsius. The solution was subjected to stirring for 2 hours. Additionally, a solution containing two weight percent of chitosan (CS) was prepared by dissolving CS in a solution consisting of 2 weight percent acetic acid. The PVA/C S ratio is determined by blending both solutions in a weight ratio of 80-20 wt% and then adding ZnO NP as three concentrations (0.2, 0.4 and 0.6 g). The solution is subjected to continuous magnetic stirring for 2 hours, and the last step for blending is using an "ultrasonic homogenizer" Table 1, which illustrated details of the composition of samples. The electrospun fibers were synthesized using this specific blend [12].

Pumping a polymer solution into a needle gauge 18 with a 10 ml syringe will make this membrane. The voltage is between 18 kV. The temperature was 22 degrees Celsius for the electrospinning process. The distance from the tip to the collector is set at 12.5 cm. 0.5 ml/h of flow was used, and spinning at 10 cm and kv for 120 minutes, respectively, was done. Before further investigation, the produced nanofibers were allowed to dry at ambient temperature for at least 24 hours and removed from the substrate.

Table 1: Sample code and their corresponding compositions

No.	of sample	PVA(%)	CS(%)	ZnO (g)
1	PVA/CS	80	20	0
2	(PVA +CS)+0.2 ZnO	80	20	0. 2
3	(PVA+CS)+0.4 ZnO	80	20	0. 4
4	(PVA +CS)+0.6 ZnO	80	20	0. 6

2.3 Characterization of nanostructures and electro-spun fibers

The optical and structural characteristics of the (CS+PVA) and (CS+PVA) +ZnO NPs samples have been examined by FTIR, as well as their morphological characteristics by FESEM, Energy Dispersion X-ray spectroscopy An EDX, Antimicrobial activity, Cell viability, Contact angle measurement, and their mechanical parts by nanoindentation.

2.3.1 Fourier transform infrared spectroscopy (FT-IR)

To verify the functional groups and bonds of polymers, an FT-IR spectrophotometer (Bruker, Germany) was employed in the inspection laboratory/material engineering department laboratory/University of Technology, and the data were analyzed using the IR Solution software (version 1.21).

2.3.2 Morphology characterization by field emission scanning electron microscopy FESEM and Energy Dispersion X-ray spectroscopy an EDX

Field emission scanning electron microscopy (FE-SEM-Imaging-EDS-Mapping-Line-EBSD/Germany) In Islamic Azadd University of Technology/Iran, an instrument is employed to examine the morphology of the scaffolds after their fabrication. Before being analyzed using Field Emission Scanning Electron Microscopy (FESEM) at an accelerating voltage of 15 kilovolts (Kv), the specimens underwent a gold plating process using sputtering, resulting in a 10 nm gold layer. The fiber diameter and pore size quantification are performed on FESEM images using the ImageJ software program.

2.3.3 Contact angle measurement

The contact angle (CA) that requires one drop of water to settle on a lotus leaf tends to be greater than 160 degree. Since ancient times, the word "hydrophobic" has been applied to describe a solid surface's resistance to holding liquid. Only a few industries could profit from hydrophobic surfaces, including textile, packaging, coatings, bioengineering, electrical devices, and drug delivery [13]. The Static Contact Angle is the essential characteristic for detecting super hydrophobic materials, which is the angle a liquid makes with a solid. The surface is hydrophilic if the water static contact angle (CA) is less than 90 degrees, hydrophobic if it is between 90 and 150 degrees, and super hydrophobic if it is greater than 150 degrees [14].

2.3.4 Antimicrobial activity

Samples 1 to 4's antibacterial effectiveness is evaluated against gram-negative and gram-positive bacterial strains using the agar well diffusion assay In Phi Nano-Science Center (PNSC)/Baghdad Senaa Street [9]. A sterile Muller-Hinton (MH) agar with a volume of 20 ml is put onto Petri dishes. A sterile wire loop separates the bacteria from their respective stock cultures [10]. Following the cultivation of the organisms, sterile tips are used to create six-mm-diameter wells on the agar plates. The prepared wells are subjected to injections of the samples at different concentrations, ranging from 1 to 4. The mean diameter of the inhibition zones is determined and documented after the incubation of culture plates with samples (1-4) and test organisms at a temperature of 37 °C for 24 hours [15].

2.3.5 Cell viability

The MTT assay is used to evaluate the fibroblast vitality on the generated nanofibrous mats; the steps are as follows, carried out by Shahrood University of Technology/Iran. Under usual conditions of 37 °C and 5% CO_2, the cells were grown in DMEM media supplemented with 10% fetal bovine serum and 1% penicillin/streptomycin antibiotic. Each experiment was conducted three times for the 24-hour, 48-hour, and 72-hour culture durations. Several experiments were carried out to improve the assessment of biocompatibility. Firstly, we assessed the cytotoxicity using the MTT test. Subsequently, we evaluated the vitality and cell proliferation using the cell counting kit-8 (CCK-8) method, utilizing fibroblast (L929) cells. The CCK-8 assay demonstrates higher sensitivity than other tetrazolium salts, such as MTT, MTS, or TXT. This type of analysis enables the utilization of colorimetric assays that are more sensitive in determining the quantity of live cells in proliferation assays and assessing cytotoxicity [16].

2.3.6 Mechanical properties

Nano-indentation experiments are performed using the Hysitron TriboLabs Nano mechanical test apparatus to analyze the mechanical properties. For indentation tests, a two-dimensional force-displacement transducer has been used. Using this device is to calculate values. Numerous indentation points distributed on the surface of the samples are carefully selected using an optical microscope. At least 5 measurements were acquired per sample; the indentation test involved only loading under force-controlled conditions with continuous measurement of load and depth [17]. Before using any experimental techniques, the calibration is performed on fused silica, a standard material, to determine the tip radius (tip area function). This test was conducted in a clean environment with a relative humidity of 45% and an ambient temperature of 23 °C [13].

2.4 Design of experiments

Four characteristics have been identified to have a significant impact on the mechanical properties of (PVA+CA)+ZnO: reinforcement content (g), stiffness content (µN/nm), max force (µN), and max depth (nm). A four-level Taguchi model is used to optimize these parameters, and the effect of their presence on Hardness was evaluated. Table 2 presents an overview of the four parameters and their related answers. The values for the parameters are assigned based on the findings of a preliminary investigation. To assess each variable's impact on Hardness, the signal-to-noise (S/N) ratios were computed for each factor.

An ANOVA is used to determine the significance of the factors impacting Hardness with a 95% confidence level. Minitab 20 is used to carry out the Taguchi technique-based optimization process. The experiment is designed using Taguchi's Orthogonal Array (Taguchi-OA), which included level 4 and parameter 4 combinations and required sixteen runs.

Table 2: Experimental parameters (factors) and their levels

Level	Reinforcement content (g)	Contact stiffness (µN/nm)	Max force (µN)	Max depth (nm)
1	0.8225	0.8050	0.6275	1.2750
2	0.7750	0.7775	0.6750	0.7550
3	0.8550	0.8250	0.8750	0.6750
4	0.6275	0.6725	0.9025	0.3750

3. Results and discussion

3.1 Fourier-transform infrared (FTIR) analysis

Figure 1 shows the FT-IR spectra of PVA, CS, and CS/PVA. As depicted in Figure 1, PVA shows a broad peak of the –OH and $–NH_2$ stretching vibration from 3490 to 3150 cm^{-1}. The peak at 2325 cm^{-1} was due to the presence of alkyl –C-H and –N-H groups; the peaks at 1525 cm^{-1} and 1550 cm^{-1} confirm the –C-O stretching and –N-H bending vibrations of amide I and amide II, respectively; the peak at 1390 cm^{-1} represents the –C-H bending vibrations; the peak at 1322 cm^{-1} was due to the presence of –the C-N stretching vibration of amide III; the peak at 1100 cm^{-1} shows a –C-O-C stretching vibration of the glycosidic linkage, and the peak around 750 cm^{-1} indicates the crystallinity in CS. The FT-IR spectrum of CS/PVA blended films shows broadband at 3250–3085 cm^{-1}, which is less in the wave numbers attributed to the –OH group in the blended film [18]. Aside from that, the alkyl group at 2925 cm^{-1} and peaks at 1323 cm^{-1} and 1085 cm^{-1} were observed due to the –O-H in-plane vibrations and –C-O out-of-plane bonding, respectively, along with shifting in the –N-H bending vibration, from 1500 cm^{-1} of amide II to 2350 cm^{-1} in the CS/PVA blended film illuminating the interaction between the –O-H and –N-H groups of CS with the –O-H group of PVA [7]. As shown in Figure 2, the interactions between the chitosan and PVA in the mix, namely the hydrophobic side chain aggregation and intermolecular and intramolecular hydrogen bonding, are responsible for the improved characteristics [19].

3.2 Morphological and microstructural analysis

The morphology of the fibrous structure of 80% PVA, 20% CS scaffold illustrated in Figure 3A, shows non- uniform fibrous structure with average fiber diameter equal to 48.093 nm and average pore size is 336.9 nm .

Figure 3B shows the FESEM micrographs of the PVA/CS nanofibers modification with the addition of nanoparticles from 0.2 ZnO. The fiber morphology was not altered by incorporating ZnO nanoparticles; the fibers maintained their characteristic ribbon shape with little bead flaws, and the average fiber diameter of the PVA/CS/0.2 ZnO is (57.699) nm. In contrast, the average pore size is (559.724) nm.

Figure 3C illustrates the mean fiber diameter (133.34 nm) and mean pore size (831 nm) of a PVA/CS/0.4 ZnO modification. Figure 3D illustrates the average fiber diameter of PVA/CS modification, which measures100.157 nm, and the average pore size, which measures 366.556 nm.

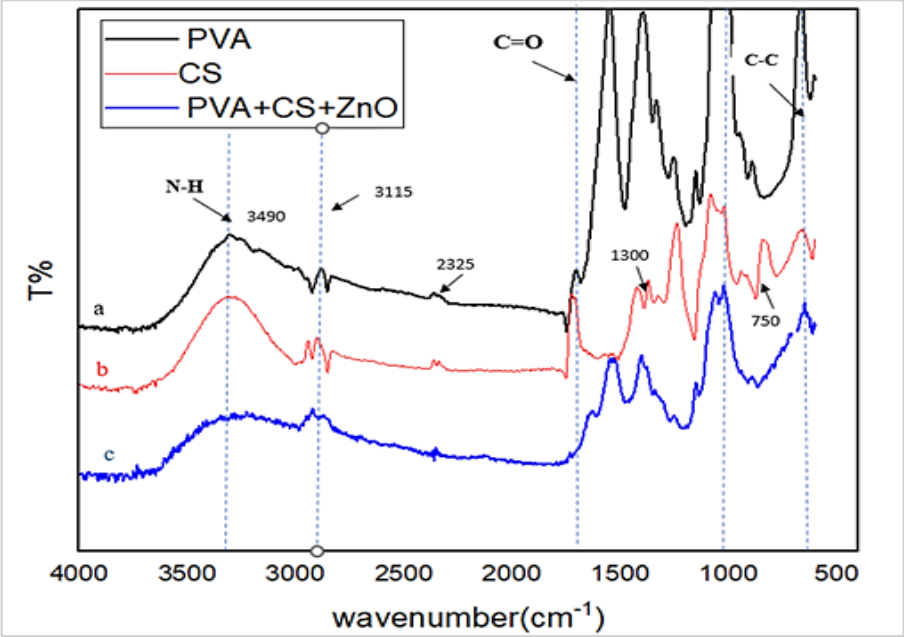

Figure 1: FT-IR spectra of pure PVA, CS, and PVA-CS-ZnO NPs electro-spun fibers

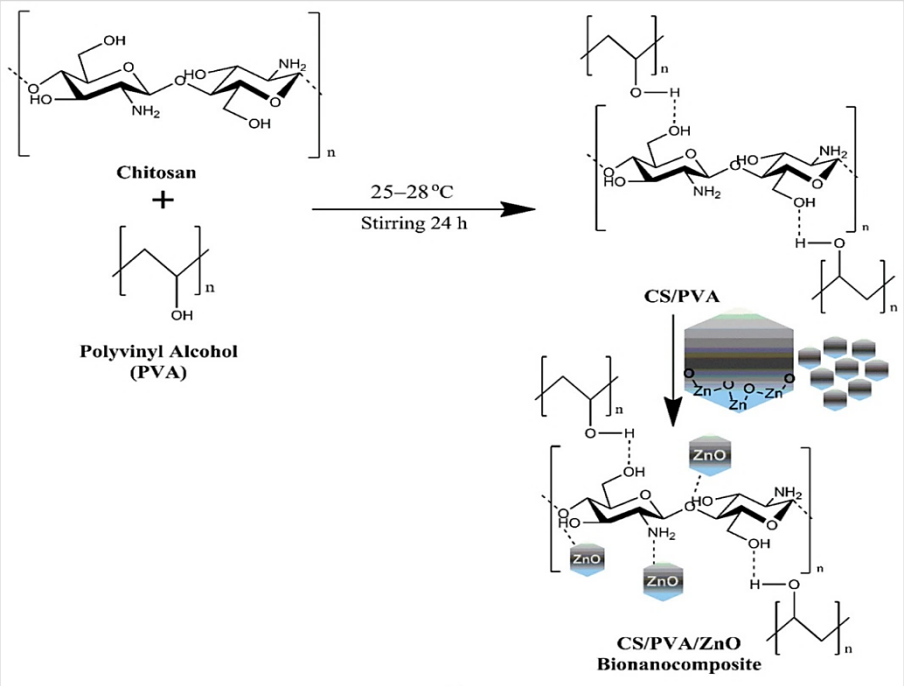

Figure 2: (CS+ PVA) +ZnO interaction [20]

In general observation, Fiber diameter, and pore size are defended according to several factors; the uneven diameter of nanofibers along different nanofiber threads is another major issue. The nanofibers' solvent coagulates when it evaporates during electrospinning. The shape and cross-section of the fiber are significantly affected by the pace of the solvent evaporation. Cross sections of nanofibers may be distorted from their ideal circular shape when sharp evaporation makes them thick, and late coagulation leads to an adhesive structure among nanofibers. The viscosity and surface tension of nanofibers in the Taylor cone area might vary greatly depending on the composition of the polymer [21]. Therefore, it is not sufficient to simply measure the diameter of nanofibers in a nanofibrous matrix, which indicates that nanofibers cannot be created in an ideal regular shape [21,22].

Scaffolds allow cell migration and proliferation because of their porous structure and linked pore network. The water vapor transfer rate (WVTR) measures a dressing's capacity to prevent moisture loss. Its hygroscopicity is also crucial and highly porous to assess a scaffold's properties for tissue engineering [21].

The FESEM images of (PVA+CS)+ZnO NPs electro-spun fibers at different magnifications are shown in Figure 3. The fibers presented a smooth surface compared to the polymer fibers without nanoparticles, average diameter of PVA/CTS/ZnO NP fibers was 100.8 nm, more significant than the average diameter of the polymer fibers without nanoparticles Figure 3A there for when the nanofiber diameter increased by increasing the weight concentration of NP because agglomeration of nanoparticles [23].

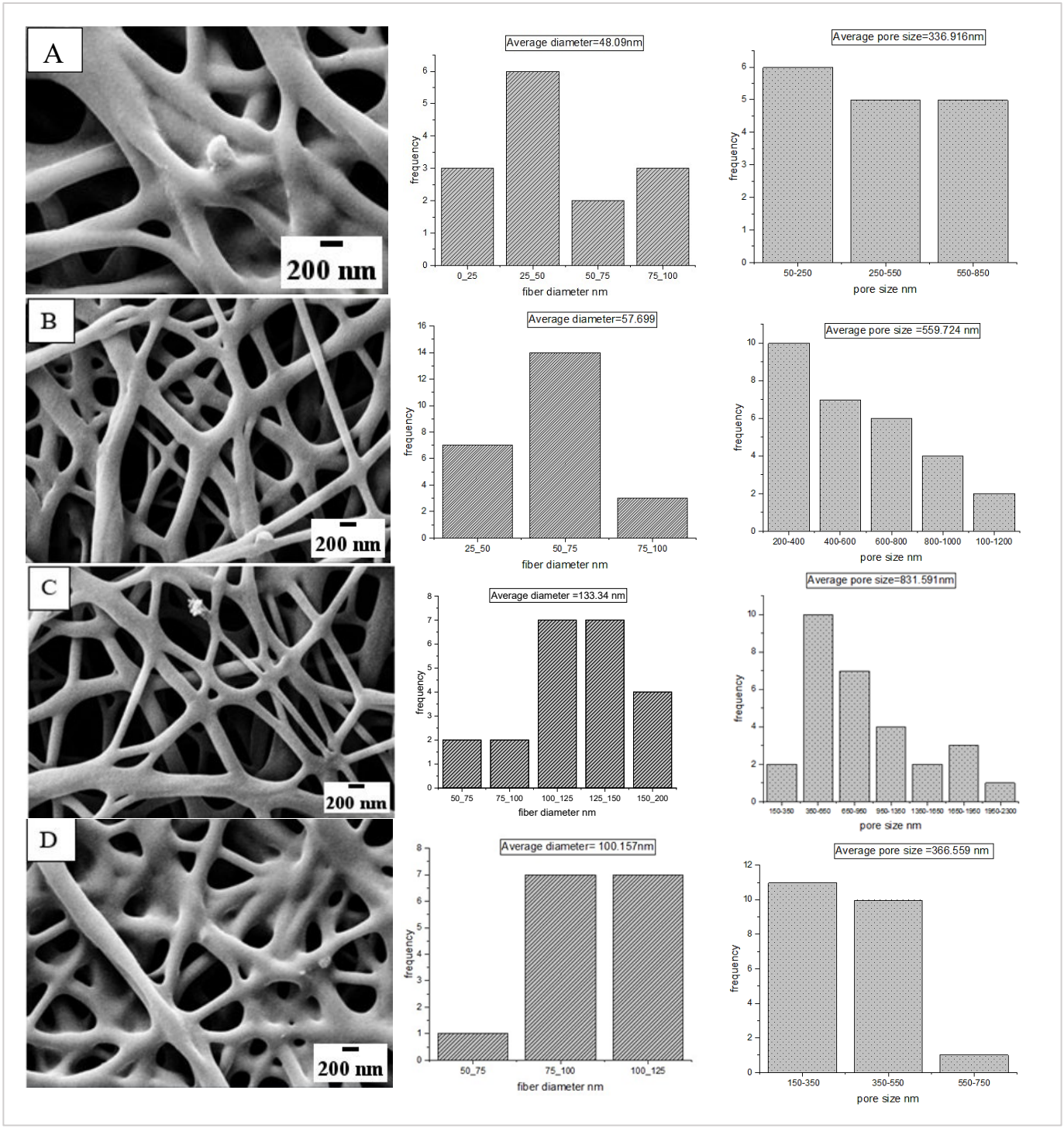

Figure 3: Fiber diameter of and pore size of:A-(CS/PVA), B-(CS/PVA)+0.2Zno,C-(CS/PVA)+0.4 Zno, D-(CS/PVA)+0.6Zno

3.3 Energy-dispersive X-ray spectroscopy (EDX)

The existence of ZnO nanoparticles within the (PVA/CS) matrix is confirmed by analyzing the EDX spectra of the (PVA/CS) and (PVA/CS/0.4 Zno) nano-composite membranes. Furthermore, it was verified that the ZnO nanoparticles reached the collector in conjunction with the polymer solution throughout the electrospinning procedure. The spectra of pristine (PVA+CS) membranes and membranes containing ZnO nanoparticles at different filler concentrations are depicted in Figure 4 in the neat (PVA + CS) case, there are distinct peaks with low energy levels that can be attributed to carbon and oxygen elements Figure

4a. However, in the composite membranes containing (PVA + CS) + ZnO, three additional peaks in Figure 4 (b,c,d) are observed at energy levels of 4.5 keV and five keV, indicative of the characteristic presence of ZnO. When employing a nanoparticle concentration of 0.2 wt.% ZnO, it is observed that the peak intensities associated with ZnO were notably diminished, with one signal at the 5 Kev level remaining undetectable. This phenomenon can be ascribed to the observation that elements present in low concentrations can produce X-ray peaks that may not be distinguishable from the background radiation. Furthermore, a notable augmentation in the magnitude of the three distinctive peaks associated with zinc and one peak corresponding to oxygen was seen as the concentration of ZnO nanoparticles was raised from 0.2% to 0.6% [4].

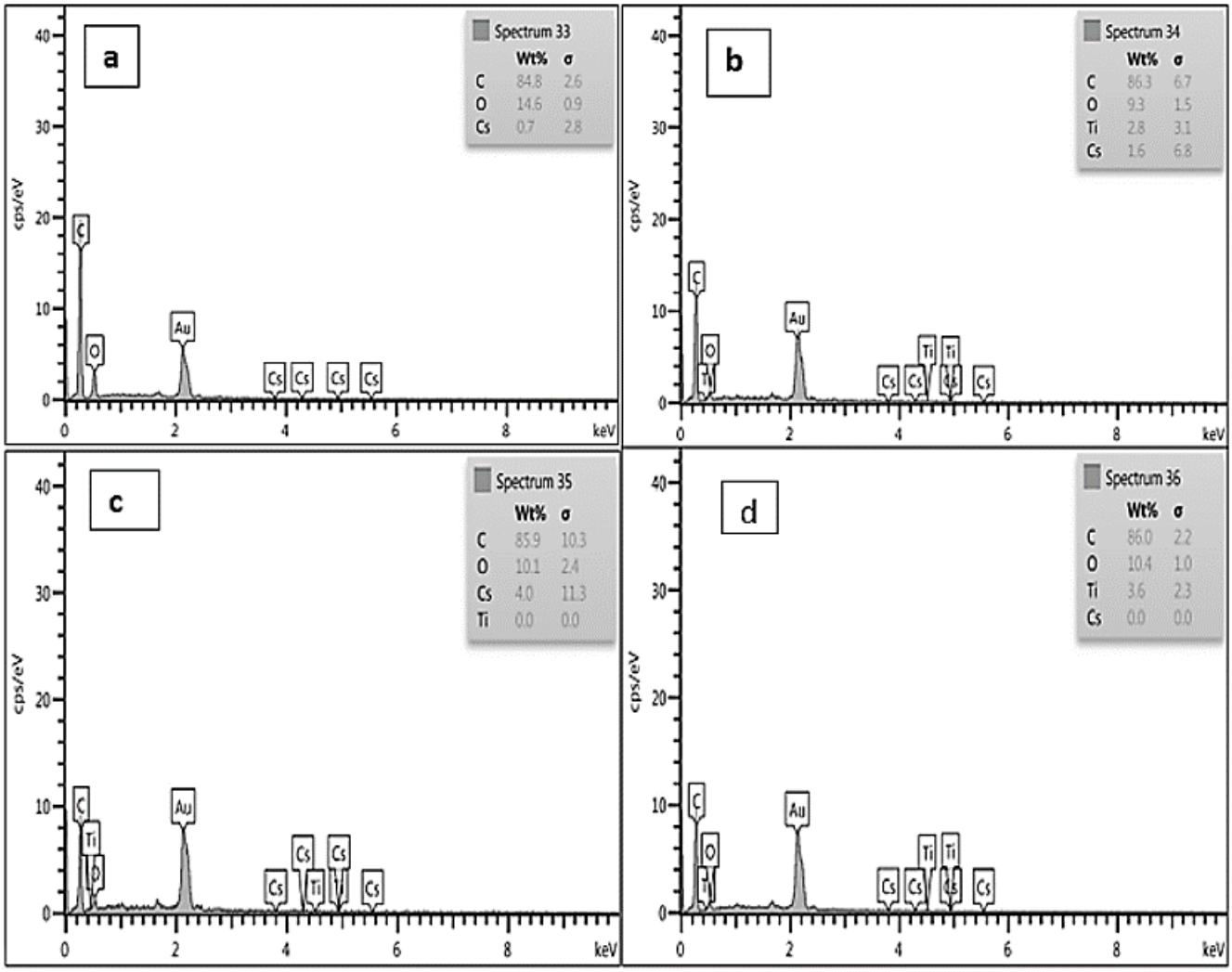

Figure 4: EDX (Energy-dispersive X-ray spectrum) of (a): (PVA + CS) membrane, (b):(PVA + CS) + 0.2 ZnO, (c): (PVA + CS) + 0.4 ZnO and (d): (PVA + CS) + 0.6 ZnO

3.4 Antibacterial activity

The data are statistically analyzed using Graph Pad Prism [16]. They are given as the mean and standard deviation (mean SD) of three separate tests, and if there is a significant difference, it is suggested at the 0.05 level (p 0.05) [14,17]. The Table 3, below present the results of antibacterial activity at various concentrations, and the related graphics give more context.

Table 3: Inhibition zone diameter for samples

The diameter of the inhibition zone as determined by the disc diffusion method		
Sample	**Inhibition zone diameter (mm)**	
	E. coli	**S. aureus**
(CS/PVA)	12	12
(CS+PVA)+0. 2 ZnO	13	13
(CS+PVA)+0. 4 ZnO	15	16
(CS+PVA)+0. 6 ZnO	18	20

The influence of inserting nanoparticles into a mixture of polyvinyl alcohol (PVA) and chitosan (CS) on the obtained antibacterial activity can be seen in Figure 5 and Figure 6. Upon observation, it is evident that all membranes in this research exhibit antibacterial activity at different levels. For example, an increase in the concentration of ZnO nanoparticles leads to an

increase in antibacterial activity. It is observed that the wound dressing materials effectively inhibit the growth of E. coli and S. aureus bacteria, leading to a major inhibitory zone after 24 hours.

In Figure 6A, the diameter of the inhibition zone for sample (a) (CS+PVA) is 12 mm when examined against E. coli and S. aureus. However, when 0.2 ZnO is added to sample (b) (CS + PVA), the inhibition zone becomes larger than that of sample (a) (CS+PVA). In Figure 6B, three samples are observed in a laboratory dish, and the inhibition zone for (CS + PVA) + 0.6 is larger than that of sample (a) (CS + PVA), which is 12 mm. In Figure 6C, (CS + PVA) + 0.6 ZnO gets to 18 mm and 20 mm when tested against E. coli and S. aureus, respectively.

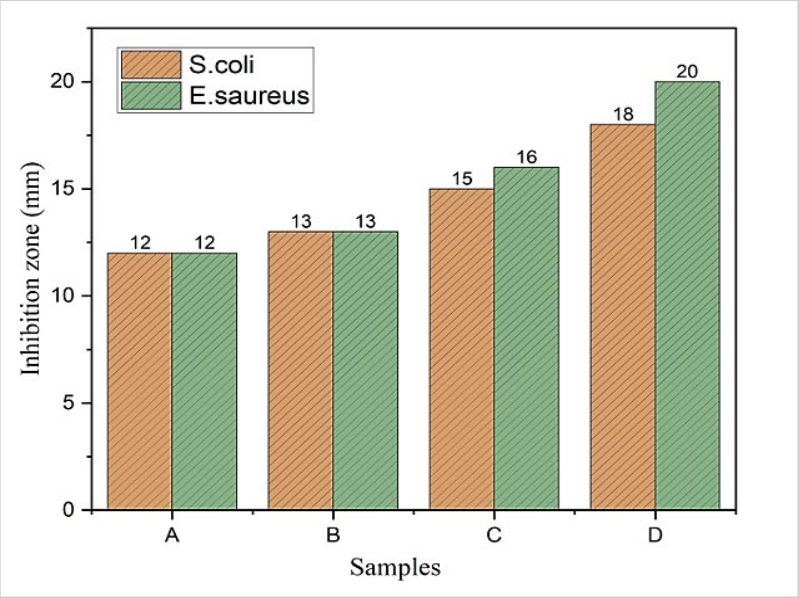

Figure 5: Effect of nanoparticle additions to (PVA/CS) on antibacterial activity for samples A:(CS/PVA), B: (CS+PVA)+0. 2 ZnO, C: (CS+PVA)+0. 4 ZnO, D: (CS+PVA)+0. 6 ZnO

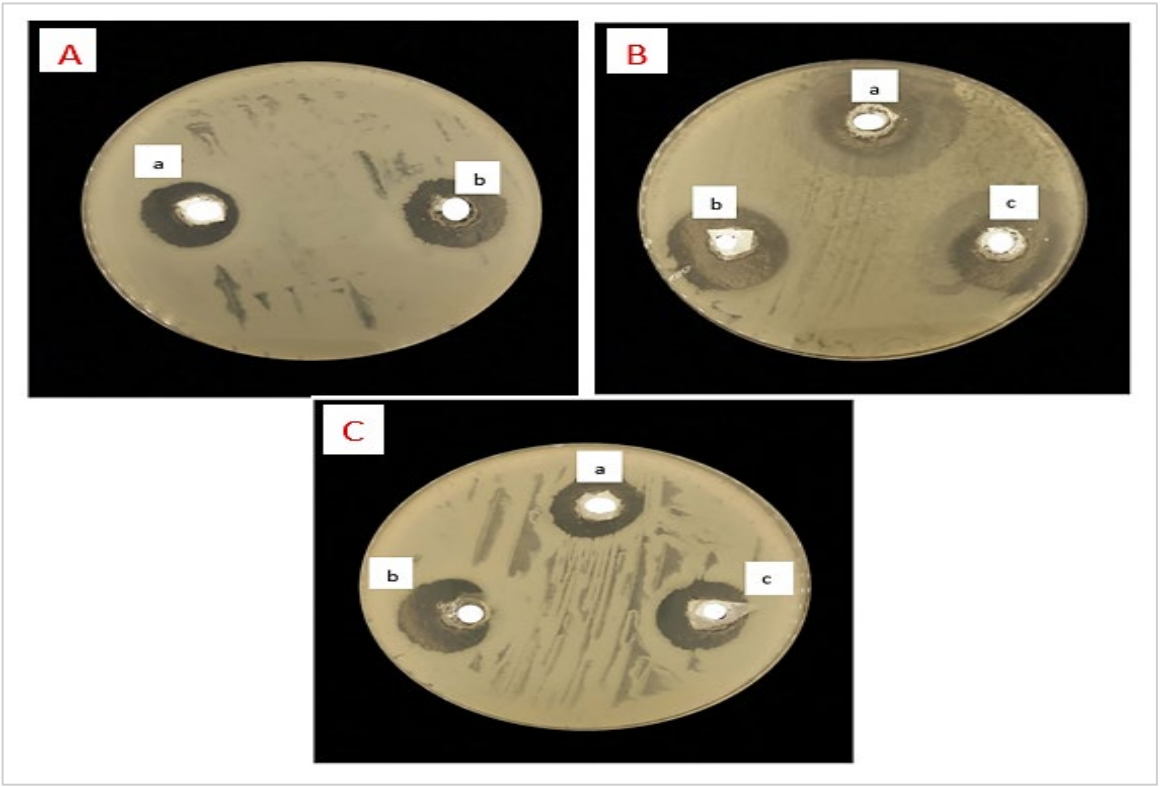

Figure 6: (A):Inhibitory zone against bacteria E. coli for a: (PVA/CS),b:(PVA+CS)+0.2 Zn, (B):Inhibitory zone against bacteria E. coli for A:(PVA+CS)+0.2ZnO, B:(PVA+CS)+0.6ZnO, C:(PVA+CS)+0.4ZnO. (C): Inhibitory zone against bacteria S. aureus for A:(PVA+CS)+0.2 ZnO, B:(PVA+CS)+0.6ZnO, C:(PVA+CS)+0.4 ZnO

3.5 Cell viability

Four samples are utilized to assess the in vitro cell proliferation using the MTT assay, which is used to count the active fibroblasts. Figure 7 shows cell viability on various nanofibrous at 24 h, 48 h, and 72 h, using empty cell culture plates as the control. Furthermore, it was discovered that L929 cells seeded on membranes had better rates of increasing and thriving than control cultures (cells cultured on the plastic surface of culture plates) and among all the manufactured composite membranes [17]. Cell viability for 24 h was over 85% at all test concentrations, demonstrating composite nanofibers' non-toxicity and good biocompatibility towards cells [18].

-For calculation of cell viability:

$$\text{Survival rate\%} = \frac{\text{AS}-\text{AC}}{\text{AC}} * 100 \quad (1)$$

where AS: Average absorbance of each sample, AC: Average control absorbance.

$$\text{Cytotoxicity rate} = 100 - \text{Survival rate} \quad (2)$$

Interestingly, after 48 hours of incubation, all cell viabilities were higher than 90% relative to the control group, and the cell viabilities of (PVA + CS) + 0.4 ZnO were higher than 100%.

3.6 Cell adhesion

The cell adhesion of L929 cells on the composite scaffolds was examined by cultivating the cells on thin scaffolds. The surface morphology of the mixed films has been examined using SEM analysis. SEM images of the dried mix films revealed a dense, quickly proliferating, nonporous surface after submerging them in a PBS solution. The culture overgrew as a result by the sixth day. The SEM surface coverage has increased throughout one, three, and five days. The L929 cells grown on the (PVA + CS) + ZnO composite scaffold and the control scaffold are observed constantly for five days [21].

The nanofibrous membrane is seen in Figure 8, SEM micrograph, which has ultra-thin fibers with sizes measured in nanometers organized randomly. The assessment of cell proliferation on the nanofibrous membranes after 1,3, and 5 days is shown in Figure 8a, which indicates a steady rise in the number of cells over the culture periods. Cells are shown sticking to the membrane surface and multiplying in Figure 8b. Remarkably, half of the surface exhibited strong contact and integration one day after cultivation. On day three, more than 70% of the area was covered Figure 8C. The membranes cultured with cells showed a confluent and covered surface after five days Figure 8D, suggesting effective cell growth and coverage [22], which means cell proliferation caused the cell to divide more. It stimulated the growth of the cell, and it increased compared to the control there after 5 days. The percentage of cells divided by 40%, as shown in Figure 8A, then became 51% in Figure 8B, then 65% and 95%, respectively, in Figure 8 C,D.

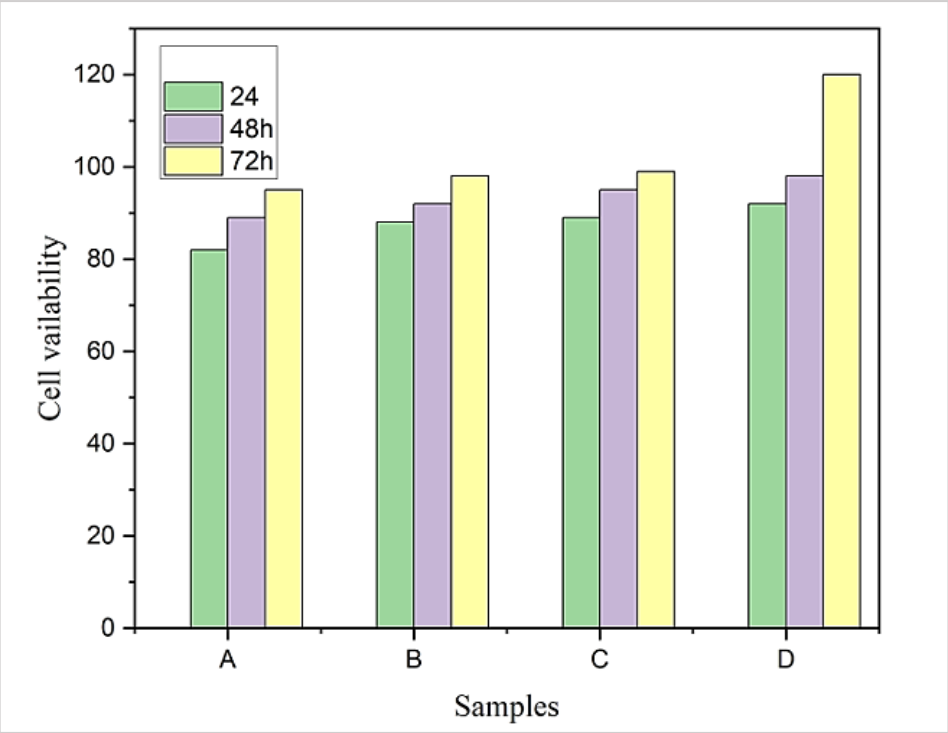

Figure 7: MTT assay for evaluating the viability of cells cultured on the samples A:(CS/PVA), B: (CS+PVA)+0. 2 ZnO, C: (CS+PVA)+0. 4 ZnO, D: (CS+PVA)+0. 6 ZnO

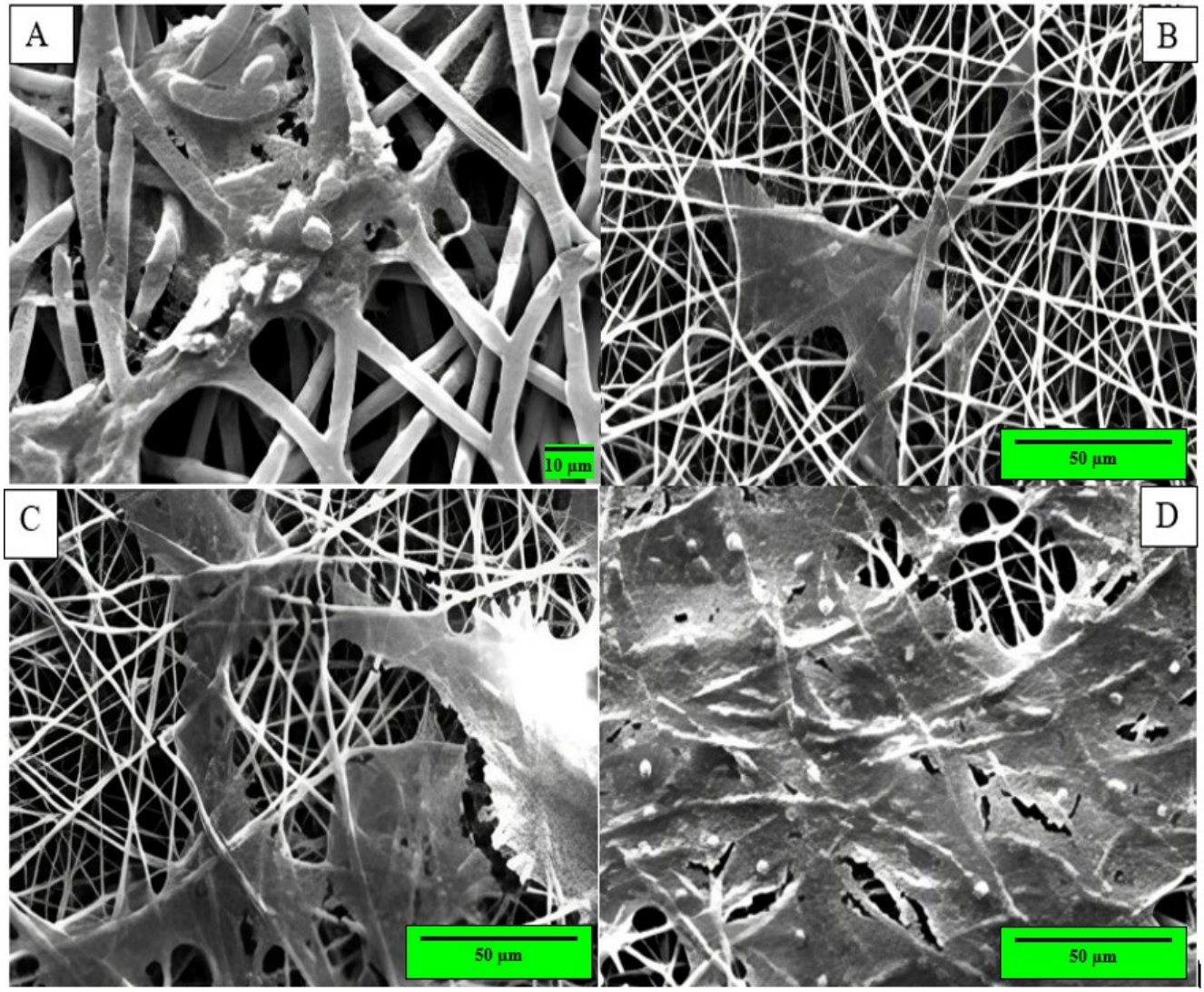

Figure 8: SEM micrographs of cells grown on the (PVA + CS) + ZnO nanofibrous membranes

3.7 Nanoindentation analysis of the samples

For the treatment of wounds, a variety of synthetic and natural polymer materials have been developed. Their poor mechanical qualities and slower water absorption rate still limit their utilization—Table 4, observes mechanical properties obtained from nano-indentation tests.

When using nanoindentation testing, that illustrated the load-unload curves for the (CS), (PVA), and (CS+PVA) in Figure 9 and the elongation-force turn, which is the same as the Stress-strain curve, can be noted By blending Cs with PVA, mechanical qualities are increased Comparing CS alone, Figure 10, the observation that adding 0.2 weight percent of ZnO increased the membrane's mechanical properties, CS+PVA membranes' mechanical properties will improve when ZnO is added [3].

Table 4: Mechanical properties obtained from the nanoindentation measurements

Sample	Er(Gpa)	Hardness(Gpa)	Contact Stiffness (µN/nm)	Max Force (µN)	Max Depth (Nm)
CS	2.9	0.05	5.5	147.2	289.3
PVA	0.5	0.02	1.3	113.6	468.7
(CS/PVA)	2.4	0.23	2.3	169.4	174.2
(PVA /CS)/0.2ZnO	9.4	0.30	8.5	177.8	127.6
(PVA/CS)/0.4 ZnO	2.1	0.12	2.8	160	219.3
(PVA/CS)/0.6 ZnO	0.3	0.07	0.6	129.5	383.9

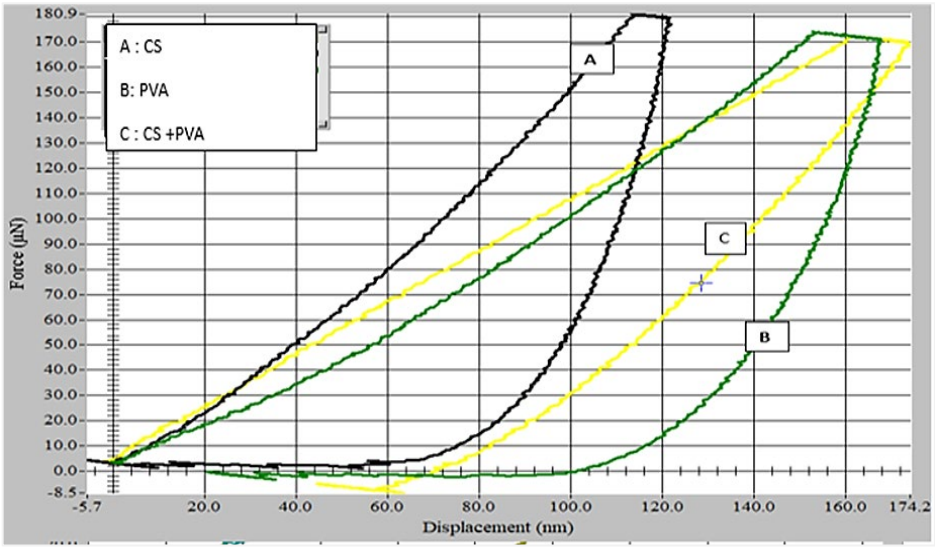

Figure 9: Load–unload curves at A: chitosan (CS). B: poly(vinyl alcohol) (PVA). C: (CS/PVA)

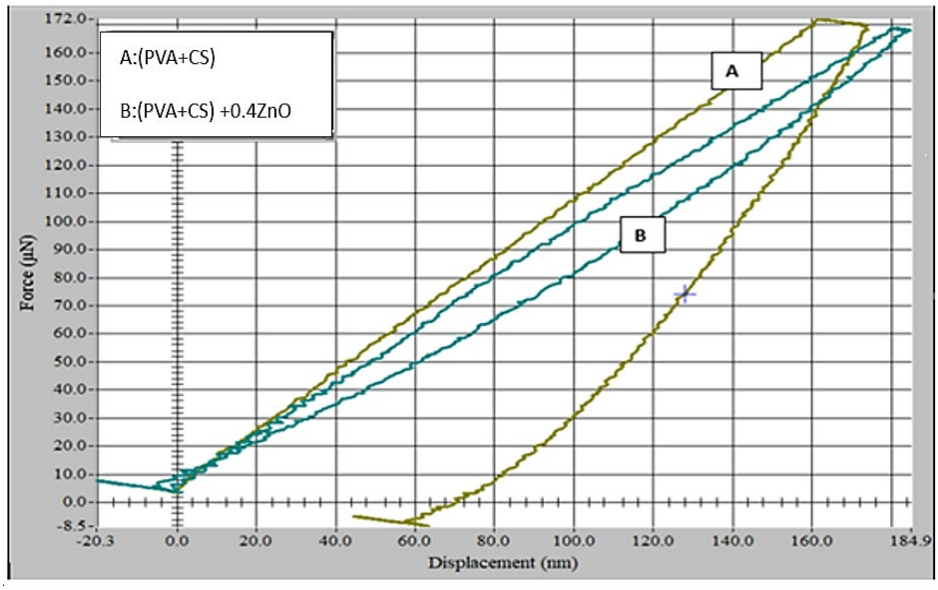

Figure 10: Load–unload curves at A**:** (CS+PVA). B**:** (CS+PVA) + 0.4ZnO

As seen in Table 4, this provides an overview of the samples' mechanical properties. It is clear that when ZnO concentration increases, the hardness of nanocomposites grows as well, peaking at 0.2 g of ZnO loading. Hardness rises to 0.3 MPa with additional ZnO content increasing, notably from 0.2 g to 0.3 g. This highlights that the degree of adhesion and dispersion between the filler and the matrix determines the mechanical characteristics of nanocomposites in the main. The ZnO nanoparticle dispersion in the (PVA+CS) matrix is remarkably uniform at smaller nanoparticle loadings. Figure 11, which shows the samples' hardness values, demonstrates this. Therefore, when the ZnO content is reduced, it is expected that there will be a homogeneous distribution of ZnO within the polymer matrix of (PVA+CS), assuming there is a more even distribution of stress, limited formation of stress-concentration sites, enhanced interfacial area for stress transfer from the polymer matrix to the fillers, and favorable mechanical properties[24,25]. The membrane's mechanical properties decrease with a high % of ZnO because when 0.2% from the ZnO nanoparticle surface, combined with the (PVA+CS) chains and integrated into the matrix, the load is homogeneously distributed between the particles with this concentration of nanoparticles the matrix more effectively limited formation of stress-concentration sites, enhanced interfacial area for stress transfer from the polymer matrix to the fillers. Favorable mechanical properties, whereas added 0.4, 0.6 ZnO nanoparticles tend to cluster inside the (PVA+CS) matrix due to these aggregated nanoparticles acting as stress concentration sites. Moreover, the aggregated nanoparticles hinder the (PVA+CS) chains' mobility, which lowers the nano composites' elongation at the break, for a high concentration of ZnO reduced mechanical properties [23].

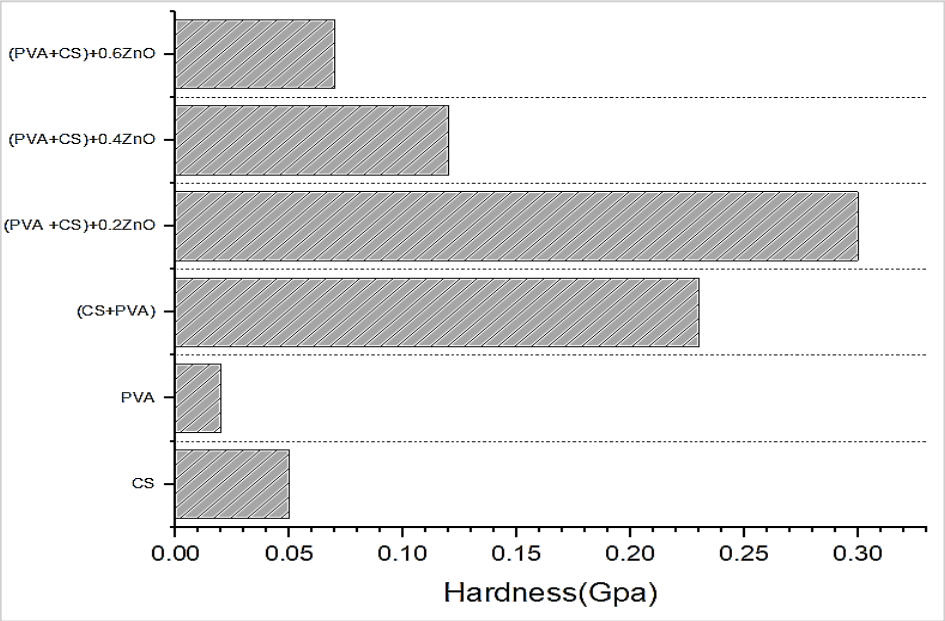

Figure 11: Hardness Values of samples

3.8 Taguchi results

3.8.1 Design of experimental (DOE)

Under the previously indicated settings, 16 experimental trials are carried out, with three replicates for each test condition. Table 5, displays the Hardness results.

The smaller-the-best criteria were used to determine the smallest hardness that could be the best condition for this study. The charts in Figure 12 determine the optimum set of parameters. From these charts, the Reinforcement (g) control factor at level 3 (0.4) gave the optimum result. While the Contact stiffness (µN/nm) control factor (2.5) gave the optimum result at level 3 (max depth (127.6 nm) at level 1, and max force (µN) at level 4 (177.8 µN) gave the optimum result, and Figure 13 shown Response optimization hardness (Gpa) [6].

3.8.2 Residual plots for response

The obtained results assess the data quality through model verification analysis. If the data follows a normal distribution, they are utilized for model verification. Alternatively, if the data does not adhere to a normal distribution, they are employed to analyze variance (ANOVA). The data quality is assessed by several statistical tests, including the normal distribution test, data independence test, and test of variance stability, as illustrated in Figure 14.

Table 5: Taguchi L16 orthogonal array of designed experiments

level	Factors				Response
	Reinforcement(g)	Contact stiffness(µN/nm)	Max force(µN)	Max depth(nm)	hardness(Gpa)
1	0	2.3	169.4	174.2	0.90
2	0	8.5	177.8	127.6	1.39
3	0	2.8	160	219.3	0.70
4	0	0.6	129.5	383.9	0.30
5	0.2	2.3	177.8	219.3	0.80
6	0.2	8.5	169.4	383.	0.40
7	0.2	2.8	129.5	174.2	0.70
8	0.2	0.6	160	127.6	1.20
9	0.4	2.3	160	383.9	0.40
10	0.4	8.5	129.5	219.3	0.50
11	0.4	2.8	169.4	127.6	1.50
12	0.4	0.6	177.8	174.2	1.02
13	0.6	2.3	129.5	127.6	1.01
14	0.6	8.5	160	174.2	0.40
15	0.6	2.8	177.8	383.9	0.40
16	0.6	0.6	169.4	219.3	0.70

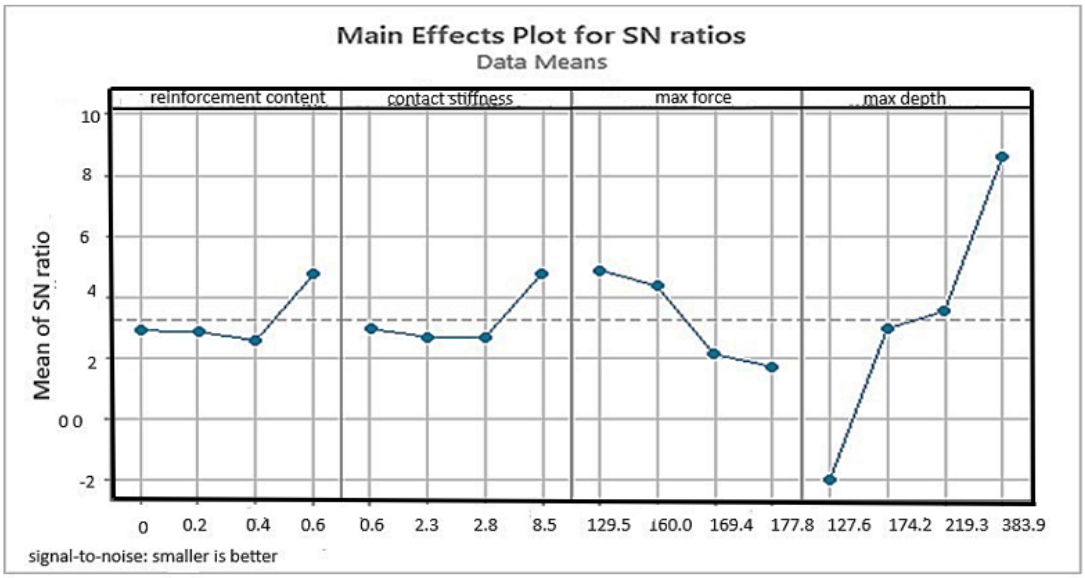

Figure 12: Taguchi analysis: main effects plot for mean of means for hardness: smaller is better

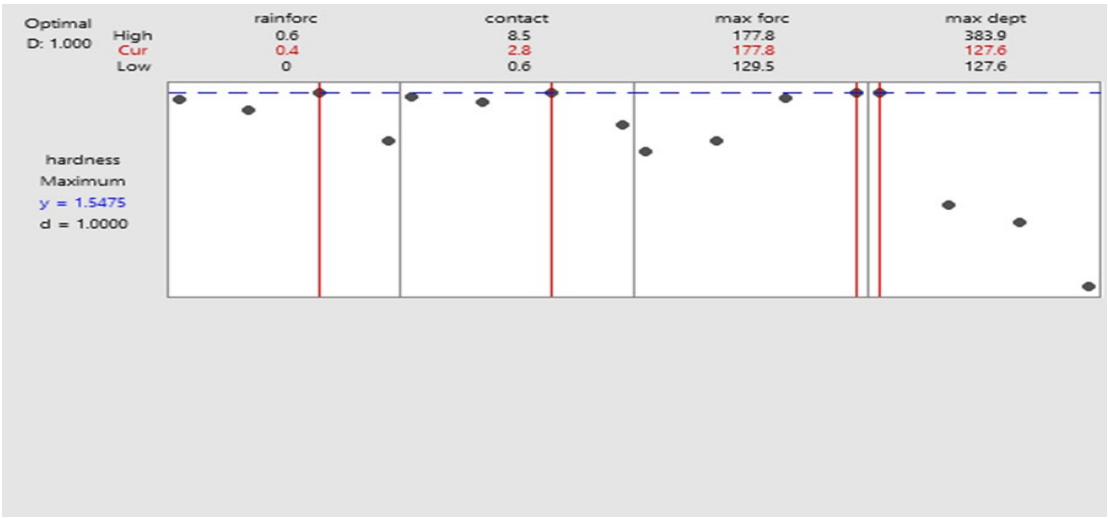

Figure 13: Response optimization hardness (Gpa)

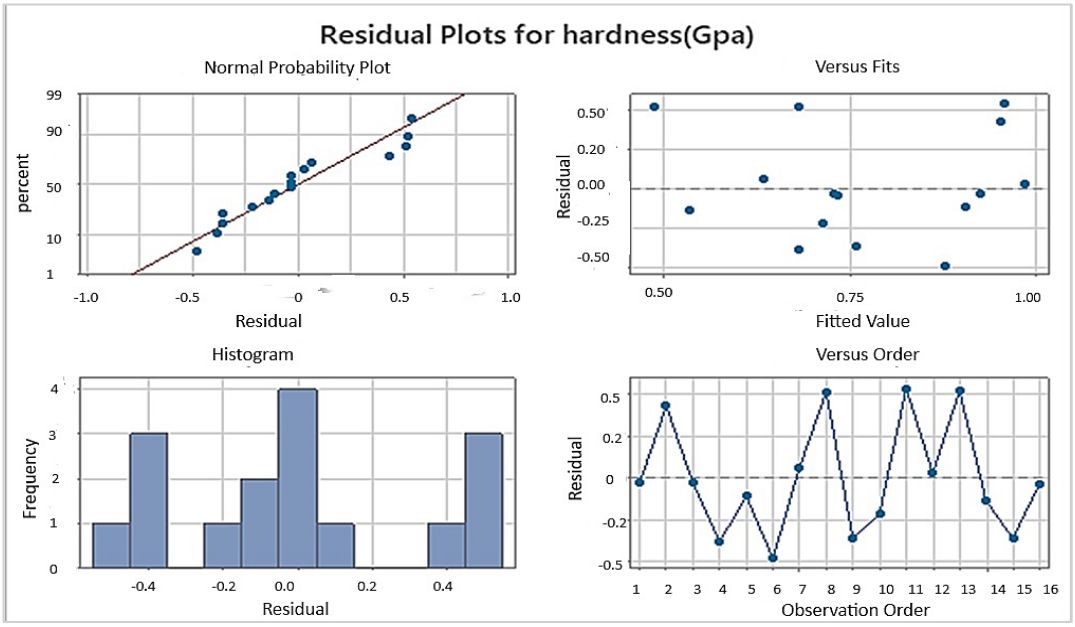

Figure 14: Residual plots for response hardness (Gpa)

3.8.3 Analysis of variance (ANOVA)

The study was done to identify the process parameters that significantly impact the response variable. The process of pooling the error sum of squares was utilized, and the ANOVA analysis was used to examine the findings of the Hardness test percentage. The factors and levels in designing a factorial design are summarized in Supplementary Table 6 shown explaine component of Equation (1).

Table 7 [26], the model created by analysis of variance (ANOVA) in Equation (1):

Regression Equation

$$\text{Hardness} = a0 + a1(x1)\text{-}(0.0) + a2(x1)\text{-}(0.2) + a3(x1)\text{-}(0.4\ ) - a4\ (x1) - (0.6) - b1(\ x2)\text{-}129.5\text{-} b2(\ x2)\text{-}160.0 + b3\ (x2)\text{-}169.4\text{-}b4(x2)\text{-}177.8 + c1\ (x3)\text{-}(0.6) + c2\ (x3)\_2.3 + c3\ (x3)\text{-}2.8\text{-}\ c4\ (x3)\text{-}8.5 + d1\ (x4)\text{-}127.6\text{-}\ d2\ (x4)\text{-}174.2 - d3\ (x4)\text{-}219.3\text{-}\ d4(x4)\text{-}383.9 \quad (1)$$

where A: reinforcement content(g), B: max force(μN), C: contact stiffness(μN/nm), D: max depth(nm)

Table 6: Component of Equation 1

Variable	Constant	Constant	Constant	Constant
A (x1)	-a0(0.7700)	-b1(0.1425)	-c1(0.0350)	-d1(0.5050)
B(x2)	- a1(0.0525)	-b2(0.0950)	-c2(0.0075)	-d2(0.0150)
D(x4)	- a2(0.0050)	-b3(0.1050)	-c3(0.0550)	-d3(0.0950)
	- a3(0.0850)	-b4(0.1325)	-c4(0.0975)	-d4(0.3950)
	- a4(0.1425)			

Table 7: Analysis of Variance

Source	DF	Adj SS	Adj MS	F-Value	P-Value	Contribution
reinforcement content (g)	3	0.72125	0.040417	17.70	0.021	38%
max force (μN)	3	0.88120	0.560400	245.43	0.000	46%
contact stiffness (μN/nm)	3	0.05525	0.018417	8.07	0.060	3%
max depth (nm)	3	0.23165	0.077217	33.82	0.8	13%
Error	3	0.00685	0.002283			
Total	15	1.88				

3.8.4 Percentage contribution

ANOVA has been performed to determine the significance of each parameter. ANOVA could provide a quantitative analysis of control factors and their effects on the properties of the final products to depict the percentage contribution of control factors on Hardness. The results of the ANOVA analysis for the Hardness show that the max force(μN)is an important factor in the process, with a contribution of 46%, followed by the reinforcement content (g) with a contribution of 38%, and max depth (nm) with (13%) but considered max stiffness not significantly factor with contribution (3%) illustrated that in Table 7. These results show that the mechanical properties or hardness are more influenced by the max force (μN) and reinforcement content (g) [27], therefore, there can be negligible max depth (nm) max stiffness from the model because no significant factor, the model becameas Equation (2):

$$\text{Hardness} = a0 + a1(x1)\text{-}(0.0) + a2(x1)\text{-}(0.2) + a3(x1)\text{-}(0.4\ ) - a4\ (x1)\ \text{-}(0.6) - b1(\ x2)\text{-}129.5\text{-} b2(\ x2)\text{-}160.0 + b3\ (x2)\text{-}169.4\text{-}b4(x2)\text{-}177.8 \quad (2)$$

3.8.5 Prediction of performance characteristics under optimum conditions

Data distribution can be effectively analyzed and modeled using a linear regression equation. Using Taguchi's orthogonal array and MINITAB software, a statistical model is developed utilizing linear regression equations. A linear regression equation is used to depict each material combination test, considering the components involved.

The linear regression Equation 1, is employed to compute the values of the response test combinations for the hardness test to estimate the expected results and percentage variation. Figure 15 displays each test's residual errors and corresponding R-square values. On the other hand, it is seen that the same set of parameters applies to the assessment of hardness response, yielding a value of 98.21%. This result suggests that the parameters are statistically appropriate for the optimization study [28] [29].

3.8.1 Response surface plot of hardness

The interactive effects of reinforcement content (g), stiffness content (μN/nm), max force (μN), and max depth (nm) are depicted in 3-D surface plots in Figure 16,17,18,19. When determining the ideal values for these variables, one important parameter to consider is the surface response. Interestingly, convex shapes are displayed by all surface plots, suggesting that the independent variables are selected with care. As indicated by a p-value < 0.05, it is found that increasing the reinforcing content

(g) and Max force (µN) significantly has affected hardness. A smaller hardness is obtained when a lower reinforcement content (g) is used. In comparison, a larger Max force (µN) was obtained at 177 µN, illustrated in Figure 16, while in Figure 17, obtained smaller hardness (0.3) with max depth (383.9 nm), Max force (129.5µN) can be obtained 0.40 Gpa, with Max force (177µN) and contact stiffness (2.8 µN/nm) this illustrated in Figure 18, in Figure 19 optimum value of hardness (0.77Gpa) vs max depth (147.9 nm), contact stiffness (2.6 µN/nm) [30].

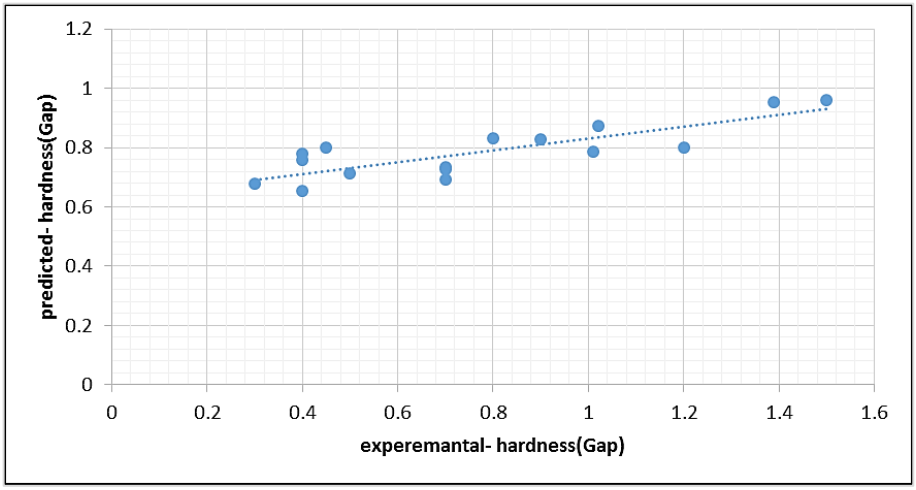

Figure 15: Regression prediction plots of hardness (Gpa)

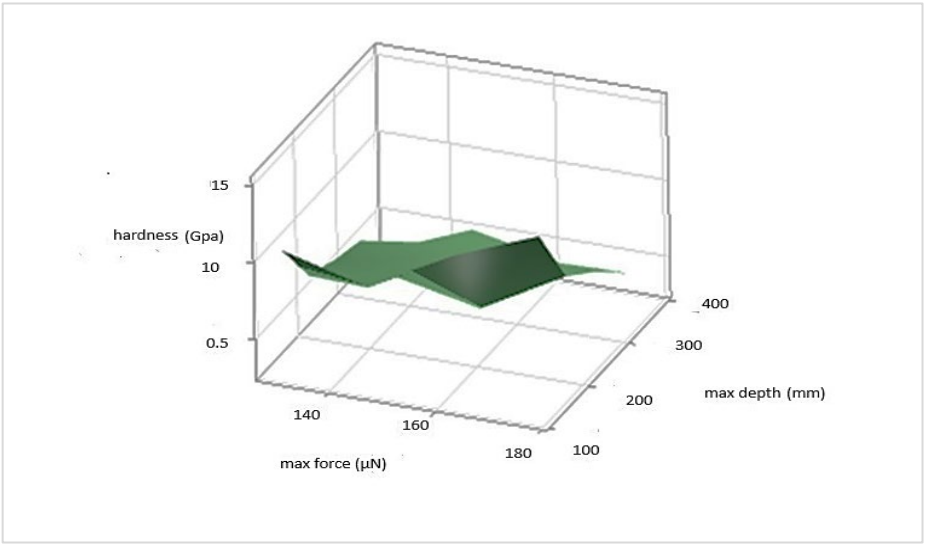

Figure 16: Surface plot of hardness vs max force , max depth

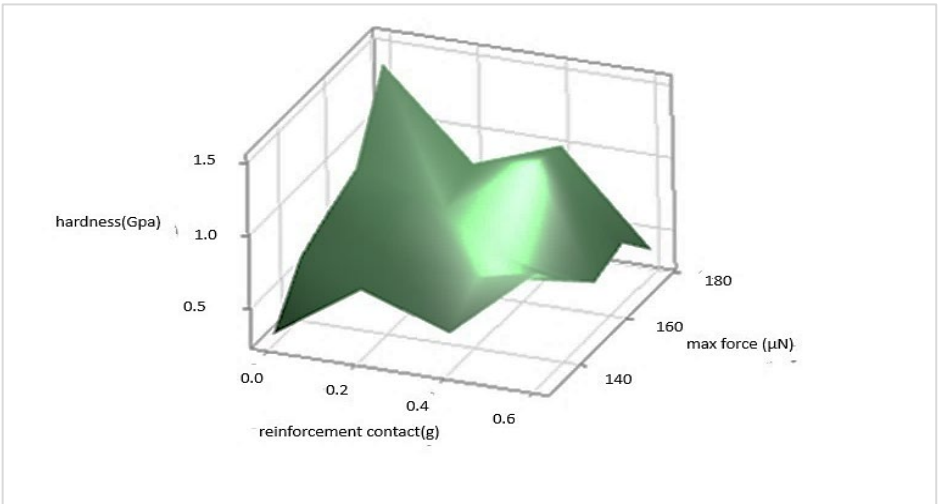

Figure 17: Surface plot of hardness (Gpa)vs reinforcement content (g), max force (µN)

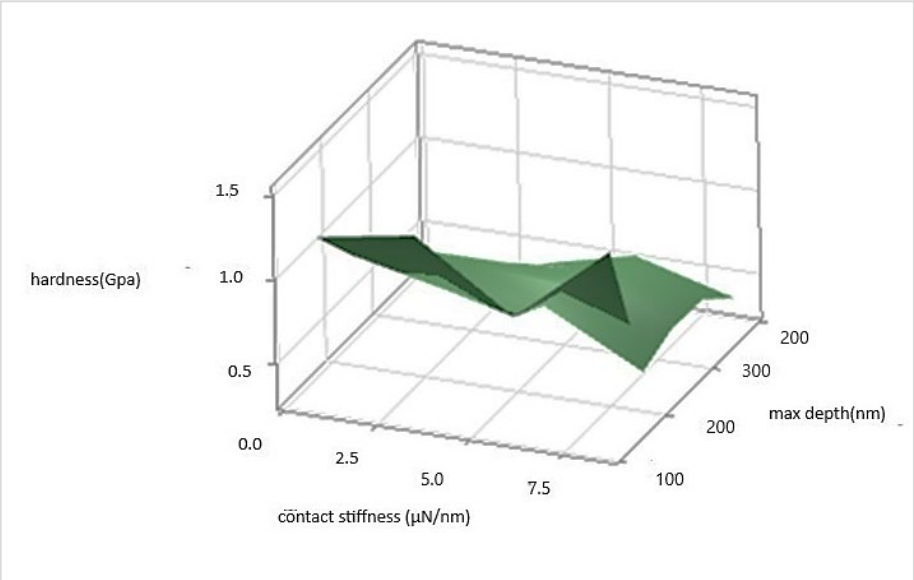

Figure 18: surface plot of hardness (Gpa)vs contact stiffness (µN/nm), max depth(nm)

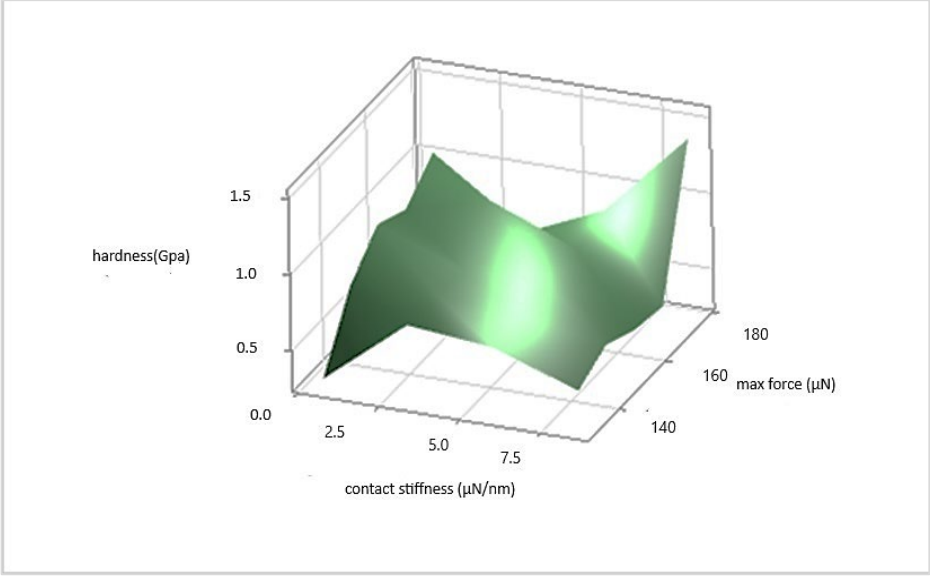

Figure 19: surface plot of hardness (Gpa) vs contact stiffness(µN/nm), max force (µN)

4. Conclusion

This investigation demonstrated the fabrication of a nanofiber membrane by the electrospinning technique, this nanofiber membrane formed by blending (80% PVA), (20% CS),and reinforced by adding (ZnO) as nanoparticles in three concentration ,the resulted shown membrane using for wound healing with good biocompatibility ,increased nanofiber to (100 nm), pore size (365 nm), Inhibition zone diameter reached to (20 mm) for (PVA + CS) + 0.6 ZnO , observation Cell viability for 24 h was over 85% at all test concentrations that's mean composite nanofibers' non-toxicity and good biocompatibility towards cells, investigated by culturing the cells on thin scaffolds After five days, the membranes that are grown with the cells have showed confluent and complete surface covering through nanoindentation test determined mechanical properties which are observed development mechanical cartelization by adding nanoparticles for obtaining composite nanofiber mat possesses significant promise as a material for wound dressings.

To identify the best-resulted qualities, the optimal possessing is chosen using the Taguchi technique when four parameters have been chosen affecting factors on mechanical properties of (PVA + CA) + ZnO, reinforcement content (g), stiffness content (µN/nm), Max force (µN), and max depth(nm), are optimized using four levels of Taguchi model, and their effect on hardness is evaluated.

The peak force (µN) is a significant role in the process, contributing 46%, according to the results of the ANOVA analysis for hardness, followed by the reinforcement content (g) with a contribution of 38%, and can be negligible max depth (nm), max stiffness from the model because not significantly factor, by this procedure, can optimize the best factor affecting on mechanical properties for preparing suitable and comfortable wound dressing materials, with Antibacterial, wound healing, biocompatible and hem compatible properties of (CS + PVA) + ZnO.

The article found that 0.2 ZnO had the best mechanical properties, whereas 0.6 ZnO had the best biocompatible properties.

When selecting a reinforcement for concentration, it is advisable to use 0.2 ZnO for a gate as it provides adequate mechanical properties for wound healing applications. Additionally, the biocompatible properties at this concentration are acceptable.

Author contributions

Conceptualization, D. Jomaa, A. Hussien and J. Dawood; methodology, D. Jomaa, A. Hussien and J. Dawood :software, D. Jomaa, A. Hussien and J. Dawood.; validation, D. Jomaa, A. Hussien and J. Dawood ; formal analysis, D. Jomaa, A. Hussien. and J. Dawood.; investigation, , D. Jomaa, A. Hussien and J. Dawood.; resources, D. Jomaa, A. Hussien and J. Dawood.; data curation, D. Jomaa, A. Hussien and J. Dawood.; writing—original draft preparation, D. Jomaa, A. Hussien and J. Dawood.; writing—review and editing, D. Jomaa, A. Hussien and J. Dawood.; visualization, D. Jomaa, A. Hussien and J. Dawood.; supervision, A. Hussien and J. Dawood.; project administration, D. Jomaa, A. Hussien and J. Dawood. All authors have read and agreed to the published version of the manuscript.

Funding

This research received no specific grant from any funding agency in the public, commercial, or not-for-profit sectors.

Data availability statement

The data that support the findings of this study are available on request from the corresponding author.

Conflicts of interest

The authors declare that there is no conflict of interest.

References

[1] A. Haider, S. Haider, and I. K. Kang, A comprehensive review summarizing the effect of electrospinning parameters and potential applications of nanofibers in biomedical and biotechnology, Arab. J. Chem., 11 (2018) 1165–1188. https://doi.org/10.1016/j.arabjc.2015.11.015

[2] M. K. A. Mohammed, M. R. Mohammad, M. S. Jabir, and D. S. Ahmed, Functionalization, characterization, and antibacterial activity of single wall and multi wall carbon nanotubes, IOP Conf. Ser. Mater. Sci. Eng., 757 (2020) 012028. https://doi.org/10.1088/1757-899X/757/1/012028

[3] S. Baghaie, M. T. Khorasani, A. Zarrabi, and J. Moshtaghian, Wound healing properties of PVA/starch/chitosan hydrogel membranes with nano Zinc oxide as antibacterial wound dressing material, J. Biomater. Sci. Polym. Ed., 28 (2017) 2220–2241. https://doi.org/10.1080/09205063.2017.1390383

[4] R. Augustine, H. Malik, D. Singhal, A. Mukherjee, D. Malakar, N. Kalarikkal and S. Thomas, Electrospun polycaprolactone/ZnO nanocomposite membranes as biomaterials with antibacterial and cell adhesion properties, J. Polym. Res., 21 (2014). https://doi.org/10.1007/s10965-013-0347-6

[5] J. Zhang, W. Xia, P. Liu, Q. Cheng, T. Tahirou, W. Gu and B. Li, Chitosan modification and pharmaceutical/biomedical applications, Mar. Drugs, 8 (2010) 1962–1987. https://doi.org/10.3390/md8071962

[6] L. Natrayan , V. Arul Kumar, S. Baskara Sethupathy, S. Sekar, P. Patil, G. Velmurugan, and S.Thanappan, Effect of Nano TiO_2 Filler Addition on Mechanical Properties of Bamboo/Polyester Hybrid Composites and Parameters Optimized Using Grey Taguchi Method, Adsorpt. Sci. Technol., 2022 (2022). https://doi.org/10.1155/2022/6768900

[7] Y. Gutha, J. L. Pathak, W. Zhang, Y. Zhang, and X. Jiao, Antibacterial and wound healing properties of chitosan/poly(vinyl alcohol)/zinc oxide beads (CS/PVA/ZnO), Int. J. Biol. Macromol., 103 (2017) 234–241. https://doi.org/10.1016/j.ijbiomac.2017.05.020

[8] M. Abbas, M. Arshad, M. K. Rafique, A. A. Altalhi, D. I. Saleh, M. A. Ayub, S. Sharife, M. Riaz, S. Z. Alshawwa, N. Masood h, A. Nazir and M. Iqbal, Chitosan-polyvinyl alcohol membranes with improved antibacterial properties contained Calotropis procera extract as a robust wound healing agent, Arab. J. Chem., 15 (2022) 103766. https://doi.org/10.1016/j.arabjc.2022.103766

[9] R. Ahmed, M. Tariq, I. Ali, R.Asghar, P. Khanam, R. Augustine and A. Hasan., Novel electrospun chitosan/polyvinyl alcohol/zinc oxide nanofibrous mats with antibacterial and antioxidant properties for diabetic wound healing, Int. J. Biol. Macromol., 120 (2018) 385–393. https://doi.org/10.1016/j.ijbiomac.2018.08.057

[10] D. Kharaghani, M. Khan, Y. Tamada, H. Ogasawara, Y. Inoue, Y. Saito, M. Hashmi, and I.Kim., Fabrication of electrospun antibacterial PVA/Cs nanofibers loaded with CuNPs and AgNPs by an in-situ method, Polym. Test., 72 (2018) 315–321. https://doi.org/10.1016/j.polymertesting.2018.10.029

[11] J. Reid, A. Donald and A. Callanan, Electrospun fibre diameter and its effects on vascular smooth muscle cells, J. Mater. Sci. Mater. Med., 32 (2021) 131. https://doi.org/10.1007%2Fs10856-021-06605-8

[12] F. Jahan, R. D. Mathad, and S. Farheen, Effect of mechanical strength on chitosan-pva blend through ionic crosslinking for food packaging application, Mater. Today Proc., 3 (2016) 3689–3696. https://doi.org/10.1016/j.matpr.2016.11.014

[13] K. Qiu and A. N. Netravali, A Composting Study of Membrane-Like Polyvinyl Alcohol Based Resins and Nanocomposites, J. Polym. Environ., 21 (2013) 658–674. https://doi.org/10.1007/s10924-013-0584-0

[14] S. Ko, J. Lee, J. Lee, B. Son, S. Jang, L. Aguilar, Y. Oh, C. Park and C. Kim., Analysis of drug release behavior utilizing the swelling characteristics of cellulosic nanofibers, Polymers (Basel)., 11 (2019). https://doi.org/10.3390/polym11091376

[15] M. A. Jihad, F. T. M. Noori, M. S. Jabir, S. Albukhaty, F. A. Almalki, and A. A. Alyamani, Polyethylene glycol functionalized graphene oxide nanoparticles loaded with nigella sativa extract: A smart antibacterial therapeutic drug delivery system, Molecules, 26 (2021). https://doi.org/10.3390/molecules26113067

[16] M. Bagheri, M. Validi, A. Gholipour, P. Makvandi, and E. Sharifi, Chitosan nanofiber biocomposites for potential wound healing applications: Antioxidant activity with synergic antibacterial effect, Bioeng. transl. med., 7 (2022). https://doi.org/10.1002/btm2.10254

[17] C. Karavasili et al., Physico-mechanical and finite element analysis evaluation of 3D printable alginate-methylcellulose inks for wound healing applications, Carbohydr. Polym., 247 (2020) 116666. https://doi.org/10.1016/j.carbpol.2020.116666

[18] M. S. Jabir et al., Inhibition of Staphylococcus aureus α-Hemolysin Production Using Nanocurcumin Capped Au@ZnO Nanocomposite, Bioinorg. Chem. Appl., 2022 (2022) . https://doi.org/10.1155/2022/2663812

[19] I. A. Kadhim, Z. J. Abdul Ameer, and A. B. Alzubaidi, Investigation of Chitosan Film Degradation in Tissue Engineering Applications, IOP Conf. Ser. Mater. Sci. Eng., 671 (2020). https://doi.org/10.1088/1757-899X/671/1/012060

[20] Z. I. Bhat, K. Imtiyaz, M. M. A. Rizvi, S. Ikram, and D. K. Shin, Comparative Study of ZnO-and-TiO2-Nanoparticles-Functionalized Polyvinyl Alcohol/Chitosan Bionanocomposites for Multifunctional Biomedical Applications, Polym., 15 (2023). https://doi.org/10.3390/polym15163477

[21] D. Semnani, 7-Geometrical characterization of electrospun nanofibers, Electrospun Nanofibers, (2017) 151–180. https://doi.org/10.1016/B978-0-08-100907-9.00007-6

[22] A. Al-Abduljabbar and I. Farooq, Electrospun Polymer Nanofibers: Processing, Properties, and Applications, Polym., (Basel)., 15 (2023). https://doi.org/10.3390/polym15010065

[23] J. Alipour, A. M. Shoushtari, and A. Kaflou, Electrospun PMMA/AB nanofiber composites for hydrogen storage applications, E-Polymers, 14 (2014) 305–311. https://doi.org/10.1515/epoly-2014-0071

[24] K. Kanimozhi, S. Khaleel Basha, V. Sugantha Kumari, K. Kaviyarasu, and M. Maaza, In vitro cytocompatibility of chitosan/PVA/methylcellulose – Nanocellulose nanocomposites scaffolds using L929 fibroblast cells, Appl. Surf. Sci., 449 (2018) 574–583. https://doi.org/10.1016/j.apsusc.2017.11.197

[25] K. Santiago-Castillo et al., Effect on the processability, structure and mechanical properties of highly dispersed in situ ZnO:CS nanoparticles into PVA electrospun fibers, J. Mater. Res. Technol., 11 (2021) 929–945. https://doi.org/10.1016/j.jmrt.2021.01.049

[26] A. Mairpady, A. H. I. Mourad, and M. S. Mozumder, Statistical and machine learning-driven optimization of mechanical properties in designing durable hdpe nanobiocomposites, Polymers (Basel)., 13 (2021). https://doi.org/10.3390/polym13183100

[27] H. A. Macías, L. Yate, E. Coy, W. Aperador, and J. J. Olaya, Insights and optimization of the structural and mechanical properties of TiWSiN coatings using the Taguchi method, Appl. Surf. Sci., 558 (2021) 149877. https://doi.org/10.1016/j.apsusc.2021.149877

[28] N. S. Muluh, N. Estella, B. Tamungang, J. N. Ghogomu, and T. D. Noufame, Pt , N co-doped TiO_2 ternary nanocomposite associated with activated carbon for the photocatalytic degradation of Methylene blue : optimization and modeling using the taguchi design, 5 (2021) 29–38.

[29] J. Zayan , A.Rasheed, A.John , M. Khalid, A. Ismail, A. Aabidand, M. Baig., Investigation on rheological properties of water-based novel ternary hybrid nanofluids using experimental and taguchi method, Mater. (Basel), 15 (2022). https://doi.org/10.3390/ma15010028

[30] R. Daassi, K. Durand, D. Rodrigue, and T. Stevanovic, Optimization of the Electrospray Process to Produce Lignin Nanoparticles for PLA-Based Food Packaging, Polym. (Basel)., 15 (2023). https://doi.org/10.3390/polym15132973